ACS APPLIED MATERIALS & INTERFACES

Research Article

www.acsami.org

Enhanced Catalytic Activity toward O_2 Reduction on Pt-Modified $La_{1-x}Sr_xCo_{1-y}Fe_yO_{3-\delta}$ Cathode: A Combination Study of First-Principles Calculation and Experiment

Wenqiang Yang,[†] Zhenbin Wang,[†] Zhiquan Wang,[†] Zhenghui Yang,[†] Changrong Xia,[†] Ranran Peng,*[,†] Xiaojun Wu,*[,†,‡,§] and Yalin Lu*[,†,‡,§]

[†]CAS Key Laboratory of Materials for Energy Conversion, Department of Materials Science and Engineering, University of Science and Technology of China, Hefei, Anhui 230026, People's Republic of China

[‡]Hefei National Laboratory of Physical Science at the Microscale, Hefei, Anhui 230026, People's Republic of China

[§]Synergetic Innovation Center of Quantum Information & Quantum Physics, University of Science and Technology of China, Hefei, Anhui 230026, People's Republic of China

Supporting Information

ABSTRACT: Using the first-principles calculation and the electronic conductivity relaxation (ECR) experimental technique, we investigated the adsorption and dissociation behaviors of O_2 on Pt-modified $La_{0.625}Sr_{0.375}Co_{0.25}Fe_{0.75}O_{3-\delta}$ (LSCF) surface. Toward the O_2 reduction, the calculation results show that the perfect LSCF (100) surface is catalytically less active than both the defective (100) surface and the perfect (110) surface. O_2 molecule can weakly adsorb on the perfect LSCF (100) surface with a small adsorption energy of about −0.30 eV, but the dissociation energy barrier of the O_2 molecule is about 1.33−1.43 eV. Doping of Pt cluster on the LSCF (100) surface can remarkably enhance its catalytic activity. The adsorption energies of O_2 molecules become −1.16 and −1.89 eV for the interfacial Fe_{int} site and the Pt_{bri} bridge site of Pt_4-cluster, respectively. Meanwhile, the dissociation energy barriers are reduced to 0.37 and 0.53 eV, respectively. The migration energy barrier of the dissociated oxygen from the interfacial Pt to the LSCF surface is 0.66 eV, and it is 2.58 eV from the top site of the Pt cluster to the interfacial Pt site, suggesting that it is extremely difficult for oxygen to migrate over the Pt cluster. The Bader charge analysis results further indicate that the charges transferring from Pt cluster to LSCF surface promote the adsorption and dissociation of O_2 molecules. Experimentally, a dramatic decrease of the surface oxygen exchange relaxation time was observed on Pt-modified LSCF cathode, with a chemical surface exchange coefficient increased from 6.05×10^{-5} cm/s of the bare LSCF cathode to 4.04×10^{-4} cm/s of the Pt-modified LSCF cathode, agreeing very well with our theoretical predictions.

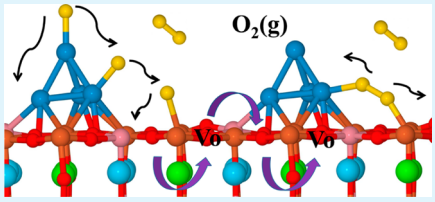

KEYWORDS: *solid oxide fuel cells, LSCF, Pt modification, oxygen reduction, density functional theory*

INTRODUCTION

Solid oxide fuel cells (SOFCs), which can effectively convert chemical fuels into electricity, have attracted increasing interests for their inherent advantages, such as high energy conversion efficiency, excellent fuel usage flexibility, and no need to use noble metal catalysts.[1−5] To achieve a satisfactory power output, SOFCs are usually needed to operate at high temperatures (~1000 °C). Unfortunately, the high operating temperature of SOFCs also brings problems such as electrode sintering and high costs of interconnect materials, which greatly hinder the commercial applications of SOFCs. Lowering the operating temperature to intermediate temperatures (IT, 500−800 °C) has become a common issue in the SOFC community. In practice, however, lowering the temperature will unavoidably result in a remarkable performance loss, mainly due to the poorer catalytic activity of the traditional cathodes, such as $La_{0.8}Sr_{0.2}MnO_{3-\delta}$ (LSM), toward the O_2 reduction at lower temperatures.[6]

Recently, some cathode materials with effective intermediate-temperature catalytic activity, such as $La_{1-x}Sr_xCo_{1-y}Fe_yO_{3-\delta}$ (LSCF),[7−9] $Ba_{0.5}Sr_{0.5}Co_{0.8}Fe_{0.2}O_{3-\delta}$,[10−12] and $Sm_{0.5}Sr_{0.5}CoO_{3-\delta}$,[13] have been explored to overcome the above problems. Among them, LSCF is a very promising cathode because of its high catalytic activity, suitable thermal expansion coefficient (TEC), and good thermal stability under normal operating conditions. For example, Rembelski et al.[10] compared the effectiveness of LSCF and LSM cathodes at the intermediate temperature with cells based on $Ce_{0.9}Gd_{0.1}O_{2-\delta}$ (CGO) electrolyte and found that the maximum power output of the cells with LSCF cathode is about 4 times higher than that with LSM at 625 °C. Gong et al. used $La_{0.9}Sr_{0.1}Ga_{0.8}Mg_{0.2}O_{3-\delta}$ as electrolyte and found that the polarization resistance of the symmetric cell using LSCF cathode is 6 orders of the

Received: September 1, 2014
Accepted: November 7, 2014
Published: November 7, 2014

magnitude lower than those with Pt and LSM electrodes.[14] Nevertheless, the native electrode performance at 500−600 °C of LSCF is still not satisfied. Interestingly, the LSCF electrode performance can be largely improved at the appearance of LSM,[15,16] Pt,[17−19] Ag,[20,21] or other noble metal particles,[22,23] although their intrinsic cathode performances are much lower when compared with LSCF. For instance, Hwang et al. reported that the polarization resistance of LSCF-0.5 vol % Pt composite electrode was nearly one-fifth of that of pure LSCF cathode at 500 °C.[8] They also found that the effectiveness of Pt adding on the LSCF electrode's performance decays with an intensive increase of Pt content and the operating temperature. Therefore, to theoretically understand the detailed mechanism would be very important for further effective cathodes design to promote the SOFCs' performance at the IT.

Theoretically, density function theory based on first-principles calculation has been proved to be a powerful tool in exploring oxygen dissociation and diffusion in SOFC's cathode at the atomic level.[24−30] Kuklja et al. demonstrated that the combined experimental and theoretical analyses of all major elementary reaction steps of the oxygen reduction could be used to predict the rate-determining steps for a given material under specific operational conditions, and thus, correspondingly, to control and improve SOFCs performance.[29] Kotomin et al. have studied the formation and migration of oxygen vacancies in (La,Sr)(Co,Fe)$O_{3-\delta}$ compounds and found that the chemical composition has little impact on the migration barrier, whereas the local cation configuration does.[31] Our previous work shows that the existence of oxygen vacancy remarkably enhance the O_2 adsorption and dissociation on (La,Sr)(Co,Fe)$O_{3-\delta}$.[32] Particularly, the increase of Co concentration in compounds could largely decrease the vacancy formation energy, and therefore accelerate the oxygen reduction. Lü et al. investigated Ag-modified $LaMnO_3$ (100) surface using a model with one Ag atom on the surface and suggested that Ag atom could promote the adsorption and dissociation of oxygen molecules over its neighboring Mn ions.[33] Until now, however, the mechanism of enhanced O_2 reduction on Pt-modified LSCF surface has not been clearly clarified in either experimental or theoretical studies.

In this work, we performed a comprehensive study on the O_2 reduction on the Pt-modified LSCF cathode (100) surface via the first-principle calculations. The calculated results indicate that the doping of Pt cluster on the LSCF surface can largely enhance the O_2 adsorption and dissociation. Moreover, the dissociated oxygen atoms at the Pt/LSCF's interface migrate easily to the LSCF surface. Experimentally, the oxygen surface exchange reaction on the Pt/LSCF cathode was investigated with the electronic conductivity relaxation (ECR) technique and the experimental results agree well with our first-principles calculation results.

METHODS

Computational Methods. All calculations were carried out using the density functional theory with the projector augmented wave (PAW) method,[34] implemented in Vienna ab initio simulation package (VASP).[35,36] The generalized gradient approximation with the Perdew−Burke−Ernzerhof (PBE) functional was used to treat the exchanging correlation effects.[37] We used the PAW potentials with valence configurations of La ($5s^25p^66s^25d^1$), Sr ($4s^24p^65s^2$), Co ($3d^84s^1$), Fe ($3d^74s^1$), O ($2s^22p^4$) and Pt ($5d^96s^1$). The kinetic energy cutoff was 400 eV, and the energy convergence criterion was 10^{-5} eV. All structures were relaxed with the Hellmann−Feynman force on each atom smaller than 0.03 eV $Å^{-1}$. Due to the negligible energy difference caused by the magnetic ordering when comparing with the adsorption energy of oxygen, ferromagnetic (FM) states were applied for all systems in order to simplify our calculations.[31,38] All calculations were spin-polarized.

The Brillouin zone integration was sampled by 2 × 2 × 1 k-points for the surface using the Monkhorst−Pack scheme.[39] The location and energy of the transition state (TS) was calculated using the climbing image nudged elastic band (CI-NEB) method.[40] Meanwhile, atomic charges were analyzed by the means of Bader charge.[41] The adsorption (E[ads]) energy of O_2 was calculated as E[ads] = E[slab + O_2] − E[slab] − E[O_2], where E[slab], E[slab + O_2], and E[O_2] are the total energies of the pristine surface, the O_2-adsorbed system, and O_2 molecule, respectively. The formation energy of oxygen vacancy (E[vac]) is defined as E[vac] = E[defect] + 1/2E[O_2] − E[perfect], where E[perfect] and E[defect] are the total energies of the prefect and defective surfaces, respectively. $La_{0.6}Sr_{0.4}Co_{0.2}Fe_{0.8}O_{3-\delta}$ is one of the most studied and promising IT-SOFC cathode materials in past experiments; therefore, we generated our models based on a similar composition $La_{0.625}Sr_{0.375}Co_{0.25}Fe_{0.75}O_{3-\delta}$ using the special quasi-random structures method (SQS).[42−45] The total electronic energy calculation manifests that the two Co atoms prefer to occupy the body diagonal position, as shown in Figure 1. The estimated lattice parameters of unit cell is $a = b = c = 3.843$ and $\alpha = \beta = \gamma = 90°$, which is in a good agreement with the experimental finding.[46]

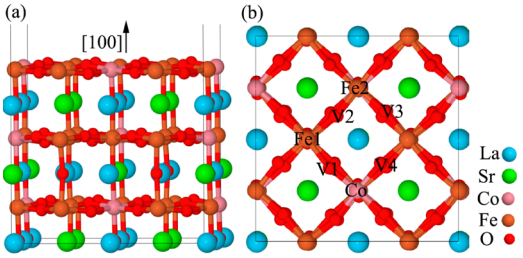

Figure 1. (a) Side and (b) top views of the perfect LSCF (100) surface.

As the (100) surface is most stable one,[28,47,48] we used a six-layer (100) slab, separated perpendicularly by a 15 Å vacuum space, to simulate the surface. The bottom three layers were fixed at their bulk position, while the atomic structures of the rest were fully relaxed. The dipole correction was applied to the direction perpendicular to the surface. To study the O_2 adsorption and dissociation, a $2\sqrt{2} \times 2\sqrt{2}$ surface slab is used. Test calculations shows that the difference of O_2 adsorption energy is smaller than 0.01 eV when using a larger 4 × 4 slab. Here, we only consider the B site terminated surface because our previous work indicated that the B sites of LSCF are more active than A sites toward oxygen reduction.[32] Figure 1 shows the side and top views of B site metal (Co,Fe) terminated perfect $2\sqrt{2} \times 2\sqrt{2}$ surface model, where Co, Fe1, and Fe2 denote three catalytically active sites for O_2 adsorption. The symbols of V1 to V4 denote the plausible locations of the surface oxygen vacancy.

To explore the O_2 adsorption and dissociation behaviors on Pt-modified LSCF surface, a Pt cluster containing four Pt atoms (Pt_4) is placed on LSCF (100) surface, as illustrated in Figure 2. Several studies suggested that the catalytic activity of Pt cluster is highly dependent on the cluster size for some types of reactions, for instance, the CO oxidation reaction.[49,50] However, this dependence is not so obvious for other reactions such as the H_2 and O_2 reaction on the Pt clusters.[51] Here, we adopt the Pt_4 cluster, which has been widely used in similar studies,[33,52−54] mainly to save the computational consumption. As depicted in Figure 2a,b, the Pt_4 cluster prefers to form a tetrahedral structure with a Fe/Co atom in the vicinity. Note that the oxygen vacancy defects are very usual on LSCF (100) surface under realistic operational conditions, the O_2 adsorption and dissociation on the defect LSCF surface was also studied. To simplify the calculation, an oxygen vacancy defect is introduced to the LSCF (100) surface, and the calculation results are summarized in the

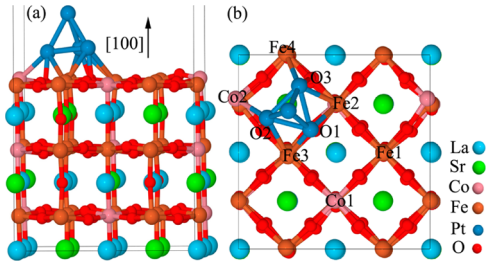

Figure 2. (a) Side and (b) top views of Pt_4/LSCF (100) surface. The atoms involved in oxygen reduction are denoted in panel b, and the atomic charges of these atoms are summarized in Table 2.

Supporting Information. It should be pointed out that the direct modeling of the oxygen reduction on the defect Pt_4/LSCF (100) surface is not explored here because a large surface model and the consequent high computation cost are needed in that case.

Experimental Methods. The oxygen surface exchange reaction on LSCF with and without Pt evaporated on surface was investigated at 775 °C, using the electronic conductivity relaxation (ECR) method. For this measurement, $La_{0.6}Sr_{0.4}Co_{0.2}Fe_{0.8}O_{3-\delta}$ powders were prepared using a solid-state reaction method. All corresponding metal oxides were mixed at the stoichiometric ratio by ball milling and calcined at 1000 °C for 5 h to form the perovskite structure. The formed LSCF powders were then cold-pressed into rectangular bars 15 mm in length, 1.06 mm in height, and 5.40 mm in width, and then sintered at 1350 °C for 5 h to form a dense sample. Pt particles were deposited onto the dense LSCF bar through vacuum evaporation (JFC-1600, JEOL) followed by heating at 900 °C for 0.5 h. The surface morphologies of LSCF with and without Pt particles were investigated using a scanning electron microscope (SEM, JSM-6700F, JEOL). The electronic conductivity relaxation method was used to examine the surface exchange properties of LSCF, as reported preciously.[55] In our relaxation process, the testing atmosphere was changed from 1% O_2–99% N_2 to air and then kept fixed at flowing air.

THEORETICAL RESULTS AND DISCUSSION

Oxygen Reduction on the Perfect LSCF (100) Surface. First, the adsorption of O_2 molecule on the perfect LSCF surface is considered. O_2 molecules adsorb on three active sites (Co, Fe1, and Fe2) forming superoxide structures, instead of peroxo-like structure. As summarized in Table 1, the adsorption energies of O_2 molecules on Fe1, Fe2, and Co sites are −0.34, −0.30, and −0.24 eV, respectively, indicating that the adsorption of O_2 molecule on Co site is slightly less stable. This adsorption behavior is similar to that on the perfect LSCF (110) surface.[32] The Bader charge analysis[41] results show that the adsorbed O_2 species obtain about 0.18–0.19 electrons from the surface, as shown in Figure 3. The charge of the oxygen atom bonding to Co atom is slightly smaller than those bonding to Fe atoms, partly resulting in the weaker bonding of oxygen species to Co sites. Note that this charge-based analysis is qualitative.

The O_2 dissociation on the perfect LSCF surface is further studied using CI-NEB method. The calculated minimum energy paths (MEPs) of O_2 dissociation are plotted in Figures 4 and 5. For the O_2 species adsorbed on Fe1 (Path 1) and Co (Path2), the dissociation energy barriers are 1.43 and 1.34 eV, respectively. These values are much larger than the adsorption energy of O_2 molecules, indicating that the dissociation of O_2 molecule on the perfect LSCF (100) surface hardly happens. The dissociation of the adsorbed oxygen on Fe2 and Fe1 sites, with a final structure in which the dissociated O atoms bonded on the two Fe atoms, was presented in Figure S1 (Supporting Information), which also proceeds with a high energy barrier (1.31 eV). The perfect LSCF (100) surface is less catalytically active for oxygen dissociation, and further modification of the surface is greatly needed in order to improve its performance.

Table 1. Adsorption Energies (E_{ads}), O–O Bond Lengths (r_{O-O}), the Atomic Effective Charges of the Adsorbed Oxygen Species on the Perfect LSCF (100) Surface, and the Pt_4/LSCF (100) Surface and the Defect LSCF (100) Surface with One Oxygen Vacancy[a]

			atomic charge (e)			
species	E_{ads} (eV)	r_{O-O} (Å)	O1	O2	O_{sum}	Pt_4
perfect LSCF(100) + O_2						
Fe1-super	−0.34	1.258	−0.17	−0.02	−0.19	
Fe2-super	−0.30	1.260	−0.16	−0.03	−0.19	
Co-super	−0.24	1.267	−0.15	−0.03	−0.18	
Fe1–Fe2-diss	0.05		−0.41	−0.36	−0.77	
Fe1–Co-diss	−0.02		−0.48	−0.44	−0.92	
Pt4/LSCF(100) + O_2						
Fe_{top}	−0.36	1.262	−0.16	−0.04	−0.20	0.57
Co_{top}	−0.38	1.264	−0.16	−0.06	−0.22	0.59
Fe_{int}	−1.16	1.336	−0.24	−0.27	−0.51	0.83
$Fe_{int-diss}$	−0.83		−0.49	−0.45	−0.94	1.10
Co_{int}	−0.79	1.286	−0.17	−0.17	−0.34	0.81
$Co_{int-diss}$	−0.77		−0.42	−0.52	−0.84	1.14
Pt_{int}	−1.89	1.383	−0.26	−0.28	−0.54	1.21
$Pt_{int-diss}$	−2.07		−0.51	−0.54	−1.05	1.66
Pt_{top}	−0.82	1.293	−0.21	−0.11	−0.32	0.90
$Pt_{top-diss}$	−1.96		−052	−0.53	−1.05	1.49
defect LSCF(100) + O_2						
Fe-super	−0.46	1.269	−0.19	−0.06	−0.25	
Fe-per	−0.69	1.374	−0.40	−0.23	−0.63	
Fe–V	−0.92	1.401	−0.54	−0.34	−0.88	
Fe-diss	−1.29		−0.99	−0.49	−1.48	
Co-super	−0.43	1.276	−0.19	−0.07	−0.26	
Co-per	−0.68	1.335	−0.27	−0.21	−0.48	
Co–V	−0.90	1.392	−0.56	−0.31	−0.87	
Co-diss	−1.25		−0.96	−0.41	−1.37	

[a]The suffix -diss denotes the final dissociated state, for example, Fe1–Fe2-diss denotes the final state of O_2 dissociation where two oxygen atoms locating on Fe1 and Fe2 (as shown in Figure 4), and $Fe_{int-diss}$ denotes the dissociated two oxygen atoms locating on interfacial Fe and interfacial Pt sites (as shown in Figure 6). The O1, O2 present the adsorbed oxygen atoms (as shown in Figure 3). The charges of the Pt clusters, denoted as Pt_4, are also listed.

Oxygen Reduction on the Pt-Modified LSCF Surface. For the Pt-modified LSCF (100) surface, several stable adsorption structures of O_2 molecules are confirmed when adsorbing on different active sites, as shown in Figure 6. Fe_{top} (Figure 6a) and Co_{top} (Figure 6b) correspond to the structures with one O atom boning to Fe and Co atom, respectively. Fe_{int} (Figure 6c) and Co_{int} (Figure 6d) denote the adsorption of O_2 molecule on the Pt-LSCF interfacial region with O atoms bonding to Fe and Pt or Co and Pt atoms simultaneously. Pt_{bri} (Figure 6e) and Pt_{top} (Figure 6f) correspond to the structures where O_2 molecule adsorbs on the bridge sites and top site of the Pt cluster, respectively. The adsorption energies (E_{ads}), O–O bond lengths (r_{O-O}) and the atomic effective charges of oxygen specie are all summarized in Table1. It is clear that the oxygen adsorption is enhanced on the Pt-modified LSCF (100) surface comparing with the perfect LSCF surface.

dx.doi.org/10.1021/am505900g | ACS Appl. Mater. Interfaces 2014, 6, 21051–21059

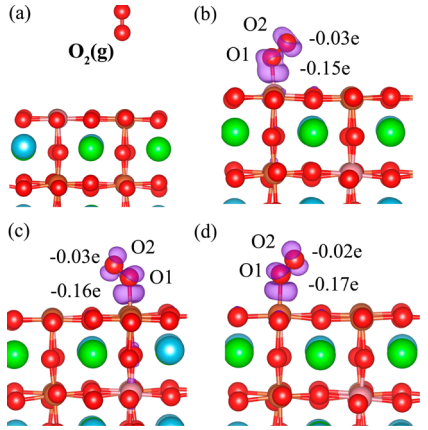

Figure 3. Charge density changes on the perfect LSCF(100) surface (a) before and after the oxygen adsorption on (b) Co, (c) Fe2, and (d) Fe1 sites. Purple indicates a charge increase, and the values in the figure are the atomic charge of the adsorbed oxygen species. $\Delta\rho_{diff}$ isosurfaces were calculated at 0.02 e/Å^3. The values are effective charges relative to those of the reactants.

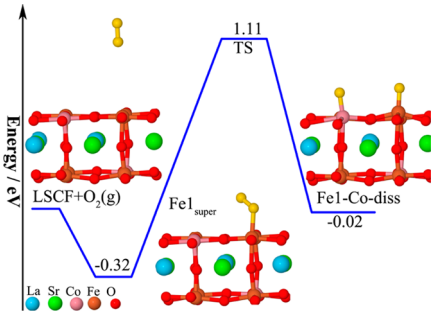

Figure 4. Dissociation energy profiles of the oxygen adsorbed on Fe1 site within the perfect LSCF (100) surface (Path1). The gold spheres are the adsorbed oxygen species.

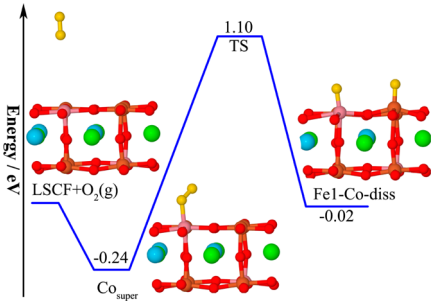

Figure 5. Dissociation energy profiles of the oxygen adsorbed on Co site within the perfect LSCF (100) surface (Path2). The gold spheres are the adsorbed oxygen species.

For the Fe_{top} and Co_{top} configurations, the adsorption energies are a little larger than those on the perfect LSCF (100) surface, indicating that the Pt modification has a minor effect on the adsorption of O_2 molecule on the top of Fe and Co atoms. Differently, the adsorption energies of O_2 molecule are −0.82, −0.79, and −1.16 eV for the Pt_{top}, Co_{int}, and Fe_{int} configurations, respectively, which are distinctly larger than those for Fe_{top} and Co_{top}. Among all adsorption configurations, the Pt_{bri} (Figure 6e) has the largest adsorption energy of −1.87 eV. Nevertheless, for the defective LSCF (100) surface without Pt cluster modification, the adsorption energy ranges from

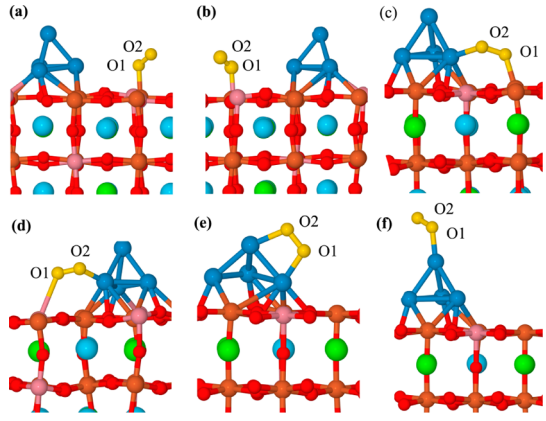

Figure 6. Geometric structures of the oxygen adsorbing on (a) Fe_{top}, (b) Co_{top}, (c)Fe_{int}, (d) Co_{int}, (e) Pt_{bri} and (f) Pt_{top} sites of the Pt_4/LSCF surface. The gold spheres are the adsorbed oxygen atoms.

−0.43 to −0.92 eV. Considering the relative weak adsorption of O_2 molecule on LSCF (100) surface, the remarkable enhancement of O_2 adsorption on the Pt cluster and the interfacial region between Pt cluster and LSCF surface is one of the possible reasons for the enhanced electrode performance of the Pt/LSCF cathode.

The MEPs of O_2 dissociation reaction on the Pt_4/LSCF (100) surface is further investigated to explore the O_2 reduction process. Here, we focus on the O_2 dissociation process in Fe_{int}, Co_{int}, Pt_{bri}, and Pt_{top} configurations for their large O_2 adsorption energies. Figure 7 displays the calculated MEPs for four considered configurations. It is shown that the whole reaction is exothermic for all four configurations. For the Fe_{int} configuration, the adsorbed O_2 dissociated into two oxygen atoms bonding to Fe and Pt atoms by overcoming an energy barrier of 0.38 eV. This value is much smaller than the adsorption energy of O_2 in the Fe_{int} configuration (−1.16 eV). The dissociation of O_2 in Co_{int} configuration proceeds with a similar energy barrier of 0.37 eV. In the Pt_{top} configuration, however, the O_2 dissociation energy barrier is as large as 1.67 eV, indicating that the dissociation of O_2 molecule in this case is very hard. For the Pt_{bri} configuration, the dissociation energy barrier of O_2 molecule is 0.53 eV, which is a little larger than those in Fe_{int} and Co_{int} configurations. Taking into account the large adsorption energy and the moderate reaction barrier, both the interfacial region (Fe_{int} and Co_{int}) and the Pt_{bri} site may play a major role in the O_2 reduction reaction on Pt-modified LSCF surface. Note that the dissociation energy barriers of O_2 molecule on Pt-modified LSCF surface are much smaller than those on the perfect LSCF, demonstrating the enhanced performance of Pt-modified LSCF. For example, the dissociation energy barrier of O_2 molecule on Fe site of perfect LSCF is 1.43 eV, about 3−4 times larger than those on Fe_{int} and Co_{int} site of the Pt/LSCF surface. It should be also noted that under realistic operational temperatures of SOFC, the entropy effect of oxygen should be considered. However, in this work, we did not consider the entropy effect,[29,56,57] mainly because the oxygen entropy effect (if dominant) should have a similar effect on all types of our cathode surfaces (perfect and defect LSCF (100) and Pt-modified LSCF (100) surface). This leads to little impact on our results that Pt cluster on LSCF surface can promote the adsorption and dissociation of oxygen molecule over LSCF cathode.

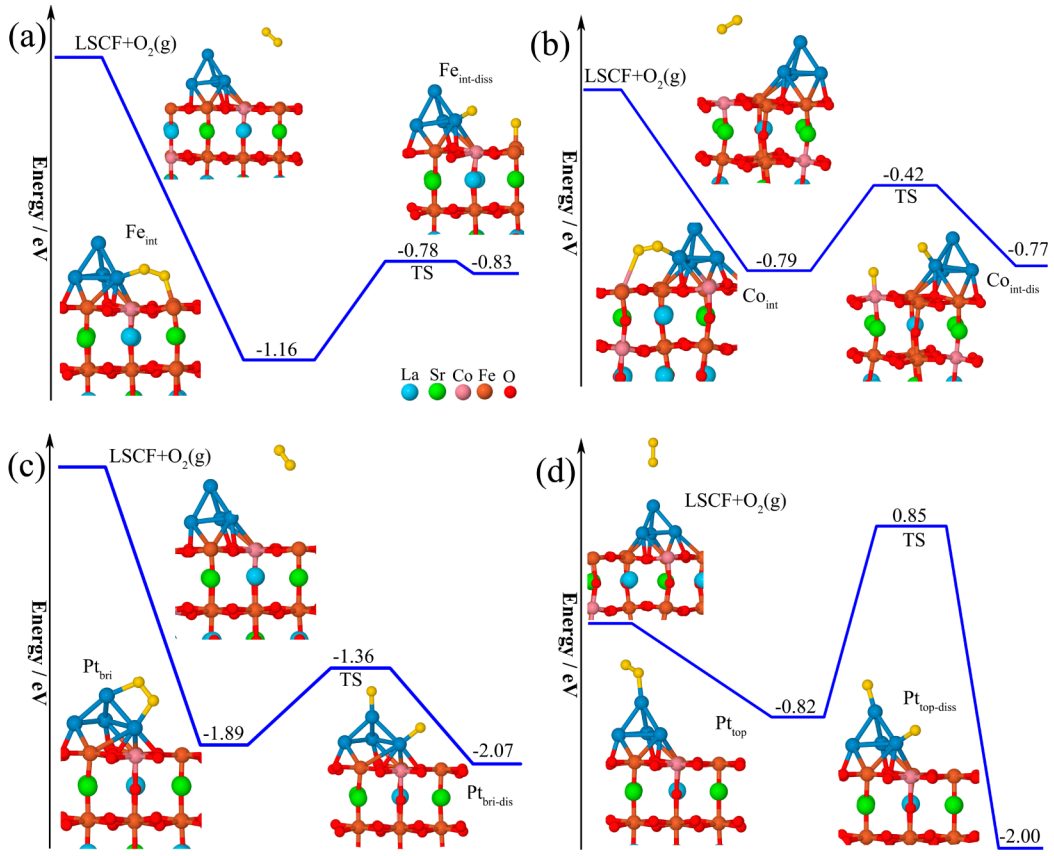

Figure 7. Dissociation energy profiles of oxygen adsorbed on the (a) Co_{int}, (b) Fe_{int}, (c) Pt_{bri}, and (d) Pt_{top} sites on the Pt_4/LSCF (100) surface.

It is well-known that the cathodic reaction for an SOFC should include the oxygen adsorption and dissociation processes, as well as the migration of the dissociated species to the electrolyte through the surface or bulk of cathode materials. Considering the continuous conducting property of the LSCF phase and the discontinuous property of Pt cluster, the migrations of dissociated oxygen species over Pt cluster and from Pt cluster to LSCF surface have to be considered, respectively. The oxygen species on Pt cluster have two typical structures in our calculations, that is, the oxygen species bonding either to the interfacial Pt (Pt1) or to the top Pt (Pt2). As shown in Figure 8, the migration of oxygen atom bonding to Pt1 (O_{int}) has a relatively low energy barrier of 0.66 eV, which is comparable to that for O_2 dissociation. However, for the oxygen species bonding to top Pt (O_{top}), two steps (O_{top}-m-1 and O_{top}-m-2) are needed to fulfill the process of migrating from top Pt to interfacial Pt with large energy barriers of 1.25 and 1.33 eV, respectively, as shown in Figure 8. The large migration energy for oxygen migrating from top Pt to interfacial Pt seems to suggest that this process is more difficult to occur compared with oxygen migration from interfacial Pt to LSCF, extremely true for a real system containing large Pt particles as defects. This result is also consistent with the experimental observation that a pure Pt cathode, which requires a dominant migration of oxygen species over the Pt surface, provides a low cathodic performance, though its adsorption and dissociation process are energetically favorable.[58,59] Fortunately, with the large energy released from the adsorption process, the difficult process is still feasible for our system with the final structure of −0.88 eV lower than the reactant.

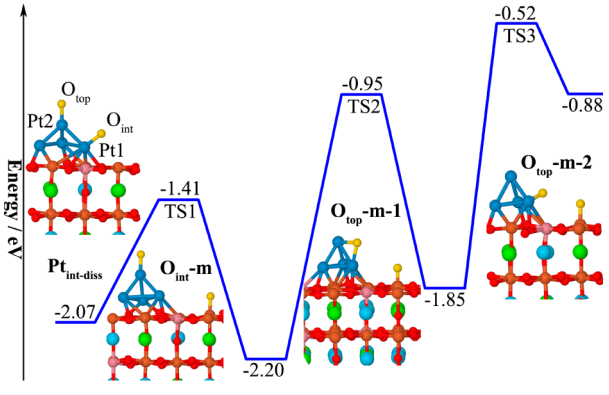

Figure 8. Migration energy profiles of the dissociated oxygen species absorbed on the Pt cluster.

To specify the migration process of oxygen species bonding to Fe or Co atoms, a model with oxygen vacancy defects is considered. As the presence of Pt cluster does not affect the bulk transportation behavior of oxygen species, here, we just use a LSCF (100) model containing oxygen vacancies to study the incorporation of dissociated oxygen species bonding to Fe or Co atoms on the LSCF (100) surface. As shown in Figure S6 (Supporting Information), the incorporation of an oxygen atom into the oxygen vacancy is energetically viable with a very low reaction barrier of 0.09−0.13 eV, and the whole reaction is exothermic, suggesting that the oxygen incorporation process would be very fast. To predict the oxygen ion migration in LSCF phase, we calculated the migration energy barriers for oxygen vacancies through LSCF (100) surface and inside its bulk. As shown in Table S1 (Supporting Information), oxygen

dx.doi.org/10.1021/am505900g | ACS Appl. Mater. Interfaces 2014, 6, 21051−21059

vacancy prefers to migrate through the LSCF (100) surface rather than through the bulk. This result is different from our previous investigation on LSCF (110) surface, where oxygen vacancy prefers to transport inside the bulk. The different surface orientation should account for such phenomena, which is similar to Kotomin's results on LSM cathode.[57] The extremely low oxygen incorporation barrier of the defect LSCF (100) surface and surface oxygen vacancy migration barrier (0.1−0.3 eV) also suggest that oxygen migration through LSCF phase is much more energetically feasible than that over Pt cluster. In short, considering the energetic profiles for oxygen adsorption, dissociation, and incorporation and the migration process over the Pt_4/LSCF surface, the most feasible reaction pathway when oxygen encounter Pt/LSCF (100) surface might contain the following steps: (1) oxygen molecules prefer to adsorb and dissociate on the Fe_{int} and Pt_{bri} sites at the interfacial region (Figure 6b,c); (2) the dissociated oxygen atoms bonding on the Fe atoms (at the interfacial region) incorporate into the LSCF surface at the presence of oxygen vacancy; (3) the dissociated oxygen species absorbed at the interfacial Pt migrate to the nearby Fe/Co atoms and then incorporate into the LSCF surface with oxygen vacancy in the vicinity; and (4) at last, the incorporated oxygen transport through the surface and bulk of LSCF to the electrolyte. Considering the large migration energy barrier (2.58 eV in total) for oxygen adsorbed on Pt_{top}, it can be deduced that the interfacial region is in fact the active area for oxygen adsorption and dissociation on the Pt/LSCF cathode. It can also be concluded that in our Pt_4/LSCF system, LSCF in fact contributes a lot to oxygen migration processes, while Pt mainly promotes the adsorption and the dissociation of oxygen gas. These results can also explain the depressed electrode performance of Pt-modified LSCF surface when Pt content exceeds a threshold.

To understand the enhanced oxygen adsorption and dissociation on Pt-modified LSCF surface, the charge difference density and the atomic charges of the involved atoms are investigated for the Pt-modified LSCF surface. As displayed in Figure 9a, a strong interaction between Pt cluster and LSCF support can be observed as electrons transferred from Pt cluster to the surface, resulting in a positive Pt cluster with the charge of 0.55 e. With the adsorption and dissociation of oxygen on a Pt cluster (interfacial or bridge sites), electrons of the Pt cluster partially transferred to the adsorbed oxygen species, leading to a more positive Pt cluster, as shown in Figure 9b−d. For example, when an oxygen molecule is adsorbed at the Fe_{int} site, 0.83 e charge is transferred from the Pt cluster to the oxygen molecule (0.51 e) and the LSCF substrate (0.32 e). In this process, the O−O bond became weakened as it enlarged from 1.234 to 1.336 Å due to the injection of electrons into the antibonding orbital of oxygen molecule. With further electrons transferring from the Pt cluster to the oxygen, the O−O bond finally broke, and about 0.94 electrons transferred in total after O_2 dissociation, of which the oxygen species bonding to Pt site was a little more negative than that bonding to Fe site, as shown in Figure 9e. Within the whole adsorption and dissociation processes, the Pt cluster lost about 1.1 e electrons in total, of which 0.20 e transferred to the LSCF substrate. Interestingly, the charge of the Fe site for oxygen adsorbing experienced a small change during this processes (ranging from 1.54 to 1.59 e), and the atomic charge of all other surface atoms, for example, Co, also underwent a negligible change, as summarized in Table 2. This result implies that the additional

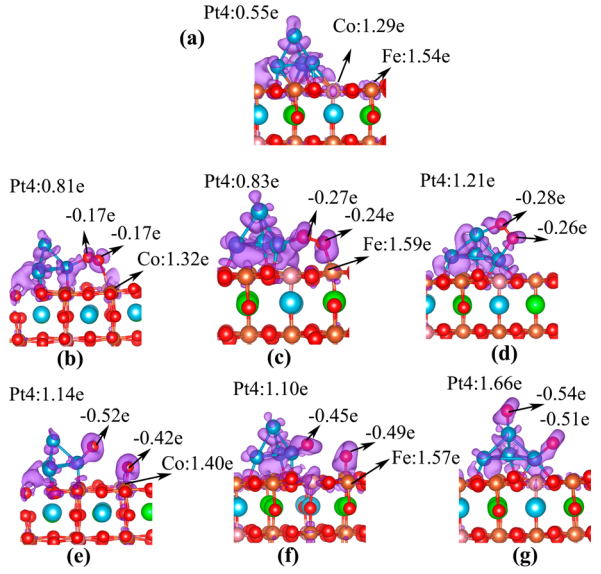

Figure 9. Charge density change of the Pt_4/LSCF (100) surface (a) before and (b−d) after O_2 adsorption, and (e−g) dissociation on(b and e) Co_{int}, (c and f) Fe_{int}, and (d and g) Pt_{bri}, respectively. The Pt4 denotes the Pt cluster. Purple indicates a charge increase, and the values in the figure are the atomic charge of the adsorbed oxygen species.

increased electrons that the oxygen obtained, compared with that on the perfect surface (Figure 3), was mainly from the Pt cluster. Therefore, the Pt cluster actually acts as an electron donator in the adsorption and dissociation processes by transferring electrons to the LSCF surface and the adsorbed oxygen, which stabilize the adsorbed oxygen and actuate the dissociation reaction as a result.

EXPERIMENT RESULTS

From the calculation results above, we can expect a greatly improved oxygen-reduction reaction on the Pt-modified LSCF surface for the much enhanced adsorption and dissociation processes, which are also vital to the oxygen surface exchange reaction. In order to experimentally verify our conclusions and to compare their oxygen surface exchange properties, we fabricated a Pt-deposited LSCF sample with vacuum evaporation technique and a bare LSCF sample.

Figure 10 shows the surface structure of bare LSCF (Figure 10a) and the surface of a Pt-deposited LSCF system (Figure 10b). As shown in Figure 10b, the Pt particles disperse relatively uniformly and are disconnected on the LSCF surface. Figure 11 shows the normalized conductivity of the two samples plotted as a function of time. The relaxation time for oxygen permeation on the bare LSCF sample is around 8000 s, while it decreases dramatically to about 1000 s on the Pt deposited LSCF sample implying a great facilitation impact of Pt. The thickness of our sample is larger than the characteristic thickness of LSCF,[60] which is usually 10−100 μm,[60−63] suggesting that oxygen permeation reaction might be limited by both surface exchange reaction and bulk transportation. Nevertheless, considering that the oxygen bulk diffusion property would hardly be impacted by surface Pt particles, the enhanced oxygen permeation property should be mainly ascribed to the much improved oxygen surface exchange reactions, involving both adsorption and dissociation reactions. Assuming that oxygen permeation was mainly surface exchange

Table 2. Charges of the Atoms That Involved during the Adsorption and Dissociation Process of Oxygen Gas over the Pt_4/LSCF (100) Surface[a]

	atomic charge (e)								
species	O1	O2	O3	Fe1	Fe2	Fe3	Fe4	Co1	Co2
perfect slab	−1.05	−1.05	−0.99	1.50	1.55	1.55	1.50	1.32	1.32
perfect slab	−1.05	−1.05	−0.99	1.50	1.55	1.55	1.50	1.32	1.32
Pt_4/Lscf	−1.03	−1.00	−0.98	1.54	1.48	1.44	1.46	1.29	1.22
Fe_{top}	−1.03	−1.00	−0.98	1.54	1.48	1.47	1.47	1.29	1.23
Co_{top}	−1.02	−1.00	−0.97	1.55	1.50	1.46	1.16	1.34	1.22
Co_{top}	−1.02	−1.00	−0.97	1.55	1.50	1.46	1.46	1.34	1.22
Fe_{int}	−1.01	−1.02	−0.97	1.59	1.55	1.42	1.51	1.33	1.30
$Fe_{int\text{-}diss}$	−0.98	−0.95	−0.97	1.57	1.48	1.41	1.52	1.35	1.29
Co_{int}	−1.03	−1.00	−0.97	1.56	1.49	1.49	1.51	1.32	1.24
$Co_{int\text{-}diss}$	−0.97	−1.00	−0.98	1.52	1.48	1.49	1.45	1.40	1.24
Pt_{bri}	−1.06	−1.02	−0.94	1.55	1.38	1.43	1.51	1.34	1.36
$Pt_{bri\text{-}diss}$	−1.06	−0.98	−0.98	1.56	1.42	1.42	1.52	1.35	1.30

[a]The atoms are denoted in Figure 2. Here, Co_{top}, Fe_{top}, Fe_{int}, Co_{int}, and Pt_{bri} indicate that O_2 adsorbed on the different sites of Pt_4/LSCF surface, as indicated in Figure 5, and $Fe_{int\text{-}diss}$, $Co_{int\text{-}diss}$, and $Pt_{bri\text{-}diss}$ indicate the final dissociated state for oxygen adsorbed on Fe_{int}, Co_{int}, and Pt_{bri}, respectively.

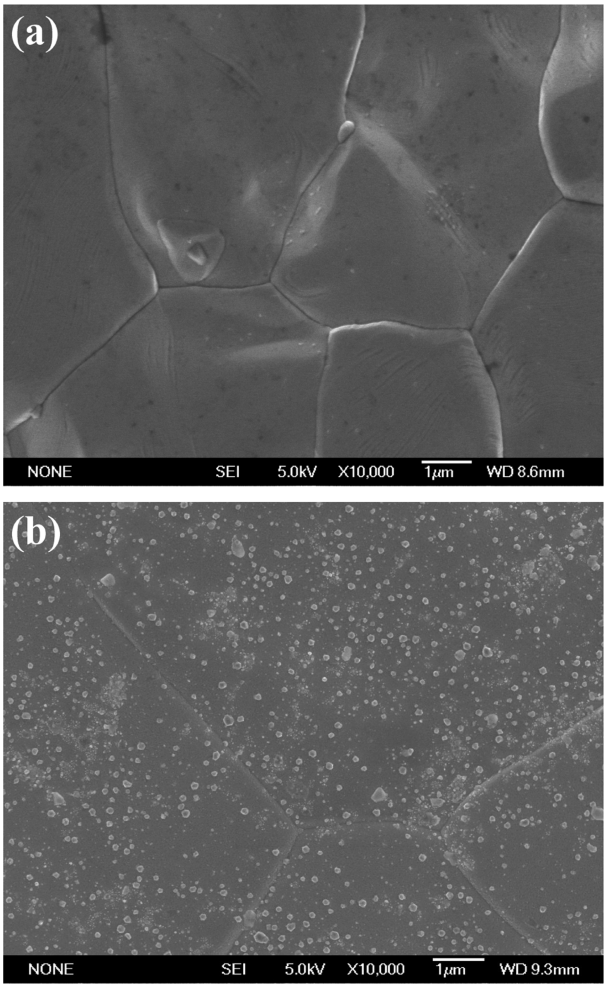

Figure 10. SEM images of (a) bare LSCF surface and (b) Pt-deposited LSCF surface.

reaction limited, the surface exchange coefficient (K_{chem}) can be fitted as 6.05×10^{-5} cm/s on the bare LSCF surface, close to the reported values ranging from 1.0×10^{-5} to 6.59×10^{-5} cm/s measured at 800 °C.[60−64] On Pt-modified LSCF surface, the fitted K_{chem} increased largely to 4.04×10^{-4} cm/s, about 6.6 times larger than that without Pt particles. Therefore, the

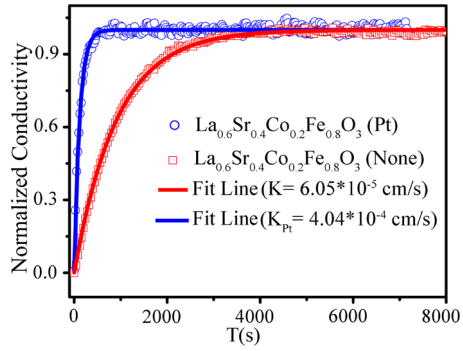

Figure 11. Normalized conductivity data and fitting curves for LSCF and the Pt-deposited LSCF samples measured at 775 °C. The fitted oxygen surface exchange coefficients of both samples are also shown.

improved reaction kinetics in our Pt-deposited sample can be attributed to the increased surface exchange coefficient (K_{chem}), as our calculation results indicated.

CONCLUSIONS

In summary, we have comprehensively studied the adsorption and dissociation of O_2 on the Pt-modified LSCF (100) surface from the first-principles insight. Adsorption and dissociation of oxygen on the perfect LSCF (100) surface can barely happen due to its low catalytic activity. With the addition of Pt to the LSCF cathode, adsorption and dissociation of O_2 are greatly enhanced. Considering the difficulty of oxygen migration on Pt cluster and the results of the charge transfer analyses of the reduction processes, we concluded that Pt mainly contributes to promote the adsorption and dissociation of oxygen gas, while LSCF contributes a lot to the oxygen migration processes. The ECR experiment results indeed demonstrate an enhanced surface oxygen exchange reaction with the deposition of Pt on LSCF, which agrees well with our calculation results. Hence, we can predict that adding materials with high electrocatalytic activity in LSCF can tremendously promote its cathodic performance.

■ ASSOCIATED CONTENT

Supporting Information

Calculation results of the O_2 dissociation between Fe1 and Fe2 sites on the perfect (100) surface, oxygen reduction on the defect LSCF (100) surface with one surface oxygen vacancy, and O atom incorporation into the oxygen vacancy. This material is available free of charge via the Internet at http://pubs.acs.org.

■ AUTHOR INFORMATION

Corresponding Authors

*E-mail: pengrr@ustc.edu.cn. Fax: 86 551 63600594. Tel: 86 551 63600594.
*E-mail: xjwu@ustc.edu.cn.
*E-mail: yllu@ustc.edu.cn.

Notes

The authors declare no competing financial interest.

■ ACKNOWLEDGMENTS

This work was financially supported by the National Basic Research Program of China (973 Program, 2012CB922001, 2012CB215403, and 2011CB921400), the National Natural Science Foundation of China (NSFC, Grant no. 51472228, 21121003), the Fundamental Research Funds for the Central Universities (Grant no. WK2060140014, WK2060190025), and the One Hundred Person Project of CAS. The authors acknowledge the Supercomputing Center of USTC, Shanghai Supercomputer Center and National Supercomputing Center in Tianjin, for providing computational resources. Figures with geometry are based on the Jmol package (Jmol: an open-source Java viewer for chemical structures in 3D. http://www.jmol.org/).

■ REFERENCES

(1) Minh, N. Q. Solid Oxide Fuel Cell Technology—Features and Applications. *Solid State Ionics* **2004**, *174*, 271−277.
(2) Yamamoto, O. Solid Oxide Fuel Cells: Fundamental Aspects and Prospects. *Electrochim. Acta* **2000**, *45*, 2423−2435.
(3) Steele, B. C. H.; Heinzel, A. Materials for Fuel-Cell Technologies. *Nature* **2001**, *414*, 345−352.
(4) Minh, N. Q. Ceramic Fuel Cells. *J. Am. Ceram. Soc.* **1993**, *76*, 563−588.
(5) Dresselhaus, M. S.; Thomas, I. L. Alternative Energy Technologies. *Nature* **2001**, *414*, 332−337.
(6) Zuo, C.; Zha, S.; Liu, M.; Hatano, M.; Uchiyama, M. $Ba(Zr_{0.1}Ce_{0.7}Y_{0.2})O_{3-\delta}$ as an Electrolyte for Low-Temperature Solid-Oxide Fuel Cells. *Adv. Mater.* **2006**, *18*, 3318−3320.
(7) Tietz, F.; Haanappel, V. A. C.; Mai, A.; Mertens, J.; Stöver, D. Performance of LSCF Cathodes in Cell Tests. *J. Power Sources* **2006**, *156*, 20−22.
(8) Hwang, H. J.; Moon, J. W.; Lee, S.; Lee, E. A. Electrochemical Performance of LSCF-Based Composite Cathodes for Intermediate Temperature SOFCs. *J. Power Sources* **2005**, *145*, 243−248.
(9) Esquirol, A.; Brandon, N. P.; Kilner, J. A.; Mogensen, M. Electrochemical Characterization of $La_{0.6}S_{0.4}Co_{0.2}Fe_{0.8}O_3$ Cathodes for Intermediate-Temperature SOFCs. *J. Electrochem. Soc.* **2004**, *151*, A1847−A1855.
(10) Rembelski, D.; Viricelle, J. P.; Combemale, L.; Rieu, M. Characterization and Comparison of Different Cathode Materials for SC-SOFC: LSM, BSCF, SSC, and LSCF. *Fuel Cells* **2012**, *12*, 256−264.
(11) Shao, Z.; Haile, S. M. A High-Performance Cathode for the Next Generation of Solid-Oxide Fuel Cells. *Nature* **2004**, *431*, 170−173.
(12) Baumann, F. S.; Fleig, J.; Habermeier, H. U.; Maier, J. $Ba_{0.5}S_{r0.5}Co_{0.8}Fe_{0.2}O_{3-\delta}$ Thin Film Microelectrodes Investigated by Impedance Spectroscopy. *Solid State Ionics* **2006**, *177*, 3187−3191.
(13) Hibino, T.; Hashimoto, A.; Inoue, T.; Tokuno, J.; Yoshida, S.; Sano, M. Single-Chamber Solid Oxide Fuel Cells at Intermediate Temperatures with Various Hydrocarbon-Air Mixtures. *J. Electrochem. Soc.* **2000**, *147*, 2888−2892.
(14) Gong, W.; Gopalan, S.; Pal, U. B. Polarization Study on Doped Lanthanum Gallate Electrolyte Using Impedance Spectroscopy. *J. Mater. Eng. Perform.* **2004**, *13*, 274−281.
(15) Ding, D.; Li, X.; Lai, S. Y.; Gerdes, K.; Liu, M. Enhancing SOFC Cathode Performance by Surface Modification through Infiltration. *Energy Environ. Sci.* **2014**, *7*, 552−575.
(16) Lynch, M. E.; Yang, L.; Qin, W.; Choi, J. J.; Liu, M.; Blinn, K.; Liu, M. Enhancement of $La_{0.6}Sr_{0.4}Co_{0.2}Fe_{0.8}O_{3-\delta}$ Durability and Surface Electrocatalytic Activity by $La_{0.85}Sr_{0.15}MnO_{3-\delta}$ Investigated Using a New Test Electrode Platform. *Energy Environ. Sci.* **2011**, *4*, 2249−2258.
(17) Uchida, H.; Arisaka, S.; Watanabe, M. High-Performance Electrode for Medium-Temperature Solid Oxide Fuel Cells: Control of Microstructure of $La(Sr)CoO_3$ Cathodes with Highly Dispersed Pt Electrocatalysts. *J. Electrochem. Soc.* **2002**, *149*, A13−A18.
(18) Uchida, H.; Arisaka, S.; Watanabe, M. High-Performance Electrodes for Medium-Temperature Solid Oxide Fuel Cells: Activation of $La(Sr)CoO_3$ Cathode with Highly Dispersed Pt Metal Electrocatalysts. *Solid State Ionics* **2000**, *135*, 347−351.
(19) Uchida, H.; Yoshida, M.; Watanabe, M. Effect of Ionic Conductivity of Zirconia Electrolytes on the Polarization Behavior of Various Cathodes in Solid Oxide Fuel Cells. *J. Electrochem. Soc.* **1999**, *146*, 1−7.
(20) Muranaka, M.; Sasaki, K.; Suzuki, A.; Terai, T. LSCF−Ag Cermet Cathode for Intermediate Temperature Solid Oxide Fuel Cells. *J. Electrochem. Soc.* **2009**, *156*, B743−B747.
(21) Sakito, Y.; Hirano, A.; Imanishi, N.; Takeda, Y.; Yamamoto, O.; Liu, Y. Silver Infiltrated $La_{0.6}Sr_{0.4}Co_{0.2}Fe_{0.8}O_3$ Cathodes for Intermediate Temperature Solid Oxide Fuel Cells. *J. Power Sources* **2008**, *182*, 476−481.
(22) Sahibzada, M.; Benson, S. J.; Rudkin, R. A.; Kilner, J. A. Pd-Promoted $La_{0.6}Sr_{0.4}Co_{0.2}Fe_{0.8}O_3$ Cathodes. *Solid State Ionics* **1998**, *113*, 285−290.
(23) Chen, J.; Liang, F.; Chi, B.; Pu, J.; Jiang, S. P.; Jian, L. Palladium and Ceria Infiltrated $La_{0.8}Sr_{0.2}Co_{0.5}Fe_{0.5}O_{3-\delta}$ Cathodes of Solid Oxide Fuel Cells. *J. Power Sources* **2009**, *194*, 275−280.
(24) Jones, A.; Islam, M. S. Atomic-Scale Insight into $LaFeO_3$ Perovskite: Defect Nanoclusters and Ion Migration. *J. Phys. Chem. C* **2008**, *112*, 4455−4462.
(25) Islam, M. S. Computer Modelling of Defects and Transport in Perovskite Oxides. *Solid State Ionics* **2002**, *154*, 75−85.
(26) Islam, M. S. Ionic Transport in ABO_3 Perovskite Oxides: A Computer Modelling Tour. *J. Mater. Chem.* **2000**, *10*, 1027−1038.
(27) Islam, M. S.; Cherry, M.; Catlow, C. R. A. Oxygen Diffusion in $LaMnO_3$ and $LaCoO_3$ Perovskite-Type Oxides: A Molecular Dynamics Study. *J. Solid State Chem.* **1996**, *124*, 230−237.
(28) Choi, Y.; Lin, M. C.; Liu, M. Computational Study on the Catalytic Mechanism of Oxygen Reduction on $La_{0.5}Sr_{0.5}MnO_3$ in Solid Oxide Fuel Cells. *Angew. Chem., Int. Ed.* **2007**, *119*, 7352−7357.
(29) Kuklja, M. M.; Kotomin, E. A.; Merkle, R.; Mastrikov, Y. A.; Maier, J. Combined Theoretical and Experimental Analysis of Processes Determining Cathode Performance in Solid Oxide Fuel Cells. *Phys. Chem. Chem. Phys.* **2013**, *15*, 5443−5471.
(30) Kotomin, E. A.; Merkle, R.; Mastrikov, Y. A.; Kuklja, M. M.; Maier, J. In *Computational Approaches to Energy Materials*;Walsch, A.; Sokol, A.; Catlow, C. R. A., Eds.; John Wiley & Sons, Inc.: Chichester, U.K., 2013; Chapter 6, pp 149−186.
(31) Mastrikov, Y. A.; Merkle, R.; Kotomin, E. A.; Kuklja, M. M.; Maier, J. Formation and Migration of Oxygen Vacancies in $La_{1-x}Sr_xCo_{1-y}Fe_yO_{3-\delta}$ Perovskites: Insight from ab Initio Calculations and Comparison with $Ba_{1-x}Sr_xCo_{1-y}Fe_yO_{3-\delta}$. *Phys. Chem. Chem. Phys.* **2013**, *15*, 911−918.

(32) Wang, Z.; Peng, R.; Zhang, W.; Wu, X.; Xia, C.; Lu, Y. Oxygen Reduction and Transport on the $La_{1-x}Sr_xCo_{1-y}Fe_yO_{3-\delta}$ Cathode in Solid Oxide Fuel Cells: A First-Principles Study. *J. Mater. Chem. A* **2013**, *1*, 12932−12940.
(33) Zhou, Y.; Lü, Z.; Guo, P.; Tian, Y.; Huang, X.; Su, W. First-Principles Study on the Catalytic Role of Ag in the Oxygen Adsorption of $LaMnO_3$ (001) Surface. *Appl. Surf. Sci.* **2012**, *258*, 2602−2606.
(34) Blöchl, P. E. Projector Augmented-Wave Method. *Phys. Rev. B* **1994**, *50*, 17953−17979.
(35) Kresse, G.; Furthmuller, J. Efficient Iterative Schemes for ab Initio Total-Energy Calculations Using a Plane-Wave Basis Set. *Phys. Rev. B* **1996**, *54*, 11169−11186.
(36) Kresse, G.; Hafner, J. Ab Initio Molecular Dynamics for Open-Shell Transition Metals. *Phys. Rev. B* **1993**, *48*, 13115−13118.
(37) Perdew, J. P.; Burke, K.; Ernzerhof, M. Generalized Gradient Approximation Made Simple. *Phys. Rev. Lett.* **1996**, *77*, 3865−3868.
(38) Mastrikov, Y. A.; Kuklja, M. M.; Kotomin, E. A.; Maier, J. First-Principles Modelling of Complex Perovskite $(Ba_{1-x}Sr_x)(Co_{1-y}Fe_y)$-$O_{3-\delta}$ for Solid Oxide Fuel Cell and Gas Separation Membrane Applications. *Energy Environ. Sci.* **2010**, *3*, 1544−1550.
(39) Monkhorst, H. J.; Pack, J. D. Special Points for Brillouin-Zone Integrations. *Phys. Rev. B* **1976**, *13*, 5188−5192.
(40) Henkelman, G.; Uberuaga, B. P.; Jónsson, H. A Climbing Image Nudged Elastic Band Method for Finding Saddle Points and Minimum Energy Paths. *J. Chem. Phys.* **2000**, *113*, 9901−9904.
(41) Henkelman, G.; Arnaldsson, A.; Jónsson, H. A Fast and Robust Algorithm for Bader Decomposition of Charge Density. *Comput. Mater. Sci.* **2006**, *36*, 354−360.
(42) Zunger, A.; Wei, S.; Ferreira, L. G.; Bernard, J. E. Special Quasirandom Structures. *Phys. Rev. Lett.* **1990**, *65*, 353−356.
(43) van de Walle, A.; Asta, M.; Ceder, G. The Alloy Theoretic Automated Toolkit: A User Guide. *CALPHAD: Comput. Coupling Phase Diagrams Thermochem.* **2002**, *26*, 539−553.
(44) van de Walle, A. Multicomponent Multisublattice Alloys, Nonconfigurational Entropy and Other Additions to the Alloy Theoretic Automated Toolkit. *CALPHAD: Comput. Coupling Phase Diagrams Thermochem.* **2009**, *33*, 266−278.
(45) van de Walle, A.; Ceder, G. Automating First-Principles Phase Diagram Calculations. *J. Phase Equilib.* **2002**, *23*, 348−359.
(46) Hashimoto, S.; Fukuda, Y.; Kuhn, M.; Sato, K.; Yashiro, K.; Mizusaki, J. Thermal and Chemical Lattice Expansibility of $La_{0.6}Sr_{0.4}Co_{1-y}Fe_yO_{3-\delta}$ (Y = 0.2, 0.4, 0.6, and 0.8). *Solid State Ionics* **2011**, *186*, 37−43.
(47) Choi, Y.; Mebane, D. S.; Lin, M. C.; Liu, M. Oxygen Reduction on $LaMnO_3$-Based Cathode Materials in Solid Oxide Fuel Cells. *Chem. Mater.* **2007**, *19*, 1690−1699.
(48) Choi, Y.; Lynch, M. E.; Lin, M. C.; Liu, M. Prediction of O_2 Dissociation Kinetics on $LaMnO_3$-Based Cathode Materials for Solid Oxide Fuel Cells. *J. Phys. Chem. C* **2009**, *113*, 7290−7297.
(49) Heiz, U.; Sanchez, A.; Abbet, S.; Schneider, W. D. Catalytic Oxidation of Carbon Monoxide on Monodispersed Platinum Clusters: Each Atom Counts. *J. Am. Chem. Soc.* **1999**, *121*, 3214−3217.
(50) Balaj, O. P.; Balteanu, I.; Roβteuscher, T. T. J.; Beyer, M. K.; Bondybey, V. E. Catalytic Oxidation of CO with N_2O on Gas-Phase Platinum Clusters. *Angew. Chem., Int. Ed.* **2004**, *43*, 6519−6522.
(51) Andersson, M.; Rosen, A. Catalytic Oxidation of Hydrogen On Free Platinum Clusters. *J. Chem. Phys.* **2002**, *117*, 7051−7054.
(52) Wang, Y. L.; Wang, Y.; Xia, C. R. Surface Process of Doped Ceria Reduction by Electrical Conductivity Relaxation. *J. Electrochem. Soc.* **2012**, *159*, F570−F576.
(53) Vajda, S.; Pellin, M. J.; Greeley, J. P.; Marshall, C. L.; Curtiss, L. A.; Ballentine, G. A.; Elam, J. W.; Mucherie, S. C.; Redfern, P. C.; Mehmood, F.; Zapol, P. Subnanometre Platinum Clusters as Highly Active and Selective Catalysts for The Oxidative Dehydrogenation of Propane. *Nat. Mater.* **2009**, *8*, 213−216.
(54) Li, J.; Croiset, E.; Sandoval, L. R. Effect of Metal Support Interface During CH_4 and H_2 Dissociation on Ni/γ-Al_2O_3: A Density Functional Theory Study. *J. Phys. Chem. C* **2013**, *117*, 16907−16920.
(55) DeBusk, M. M.; Yoon, M.; Allard, L. F.; Mullins, D. R.; Wu, Z.; Yang, X.; Veith, G.; Stocks, G. M.; Narula, C. K. CO Oxidation on Supported Single Pt Atoms: Experimental and ab Initio Density Functional Studies of CO Interaction with Pt Atom on θ-Al_2O_3(010) Surface. *J. Am. Chem. Soc.* **2013**, *135*, 12634−12645.
(56) Mastrikov, Y. A.; Merkle, R.; Heifets, E.; Kotomin, E. A.; Maier, J. Pathways for Oxygen Incorporation in Mixed Conducting Perovskites: A DFT-Based Mechanistic Analysis for (La, Sr)$MnO_{3-\delta}$. *J. Phys. Chem. C* **2010**, *114*, 3017−3027.
(57) Kotomin, E. A.; Mastrikov, Y. A.; Heifets, E.; Maier, J. Adsorption of Atomic and Molecular Oxygen on The $LaMnO_3$(001) Surface: Ab Initio Supercell Calculations and Thermodynamics. *Phys. Chem. Chem. Phys.* **2008**, *10*, 4644−4649.
(58) Vladikova, D. E.; Stoynov, Z. B.; Barbucci, A.; Viviani, M.; Carpanese, P.; Kilner, J. A.; Skinner, S. J.; Rudkin, R. Impedance Studies of Cathode/Electrolyte Behaviour in SOFC. *Electrochim. Acta* **2008**, *53*, 7491−7499.
(59) Barbucci, A.; Bozzo, R.; Cerisola, G.; Costamagna, P. Characterisation of Composite SOFC Cathodes Using Electrochemical Impedance Spectroscopy. Analysis of Pt/YSZ and LSM/YSZ Electrodes. *Electrochim. Acta* **2002**, *47*, 2183−2188.
(60) Bouwmeester, H. J. M.; Kruidhof, H.; Burggraaf, A. J. Importance of The Surface Exchange Kinetics as Rate Limiting Step in Oxygen Permeation Through Mixed-Conducting Oxides. *Solid State Ionics* **1994**, *72*, 185−194.
(61) Bouwmeester, H. J. M.; Otter, M. W. D.; Boukamp, B. A. Oxygen Transport in $La_{0.6}Sr_{0.4}Co_{1-y}Fe_yO_{3-\delta}$. *J. Electrochem. Soc.* **2004**, *8*, 599−605.
(62) Li, S.; Jin, W.; Xu, N.; Shi, J. Synthesis and Oxygen Permeation Properties of $La_{0.2}Sr_{0.8}Co_{0.2}Fe_{0.8}O_{3-\delta}$ Membranes. *Solid State Ionics* **1999**, *124*, 161−170.
(63) Lane, J. A.; Benson, S. J.; Waller, D.; Kilner, J. A. Oxygen Transport in $La_{0.6}Sr_{0.4}Co_{0.2}Fe_{0.8}O_{3-\delta}$. *Solid State Ionics* **1999**, *121*, 201−208.
(64) Hu, B.; Wang, Y.; Xia, C. Oxygen Incorporation at the Three-Phase Boundary of LSCF-SDC Composite. *J. Power Sources* **2014**, *269*, 180−188.